Comparative Analysis of Ascorbic Acid-Induced Cell Sheet Formation in HaCaT Keratinocytes and Human Dermal Fibroblasts

Hatice Demir^{1,0}, Arzu Coleri Cihan^{2,*,0}

ABSTRACT

Introduction: This study examines the effects of varying L-ascorbic acid (L-AA) concentrations and initial seeding densities on cell-sheet formation by human dermal fibroblasts (HDFs) and keratinocytes (HaCaT). Both cell types were seeded at either 50,000 or 100,000 cells cm $^{-2}$ and exposed to 0, 25, 50, or 100 µg mL $^{-1}$ L-AA. Cell-sheet formation was assessed morphologically; cell viability was quantified by an MTT assay; and gene expression was measured by qRT-PCR using newly designed primers. **Methods**: In HDF cultures, the 50 µg mL $^{-1}$ group at a seeding density of 50,000 cells cm $^{-2}$ produced the most cohesive and viable sheets, accompanied by a marked up-regulation of COL1A1, reflecting enhanced extracellular-matrix synthesis. At 25 µg mL $^{-1}$, HDF morphology and viability were similar to those of the untreated control, with no cohesive sheet formation, whereas 100 µg mL $^{-1}$ induced pronounced cytotoxicity. **Results**: In HaCaT cultures, no cohesive sheets were observed at any concentration. Nonetheless, at 50 µg mL $^{-1}$ and 100,000 cells cm $^{-2}$, confluent HaCaT monolayers displayed increased expression of keratin 14 (KRT14), involucrin (IVL), and Ki-67, indicating enhanced proliferation and early differentiation despite absent sheet integrity.

Conclusion: Collectively, these findings demonstrate that L-AA promotes sheet formation in fibroblasts but not in keratinocytes under two-dimensional monolayer conditions. The limited Ha-CaT response suggests that co-culture or three-dimensional systems may be required for epithelial stratification. This study underscores the importance of tailoring L-AA concentrations and cell densities to each cell type in skin tissue engineering.

Key words: Cell sheet, ascorbic acid, HaCaT, HDF, MTT, crystal violet, qRT-PCR

¹Ankara University, Graduate School of Natural and Applied Sciences, Department of Biology, Sehit Omer Halisdemir Boulevard, 06110, Diskapi, Ankara, Türkiye

²Ankara University, Faculty of Science, Department of Biology, 06100, Dögol Street, Tandogan, Ankara, Türkiye

Correspondence

Arzu Coleri Cihan, Ankara University, Faculty of Science, Department of Biology, 06100, Dögol Street, Tandogan, Ankara, Türkiye

Email: acihan@science.ankara.edu.tr

History

- Received: 12/06/2025
- Accepted: 20/10/2025
- Published Online: 31/10/2025

DOI: https://doi.org/10.15419/r0m74x08



Copyright

© Biomedpress. This is an openaccess article distributed under the terms of the Creative Commons Attribution 4.0 International license.



INTRODUCTION

The skin, being the largest organ in the body, plays a critical role in maintaining homeostasis, barrier function, immune responses, and tissue integrity ¹. Thanks to advanced tissue-engineering approaches, laboratory-generated three-dimensional (3D) cellular models and cell-sheet technologies show remarkable potential, especially in the fields of wound healing, regenerative medicine, and skin-disease modelling ².

Cell-sheet technology allows cells to be harvested together with their native extracellular matrix (ECM) in an integrated manner, without requiring enzymatic separation. Cellular structures created via this method provide a more physiological microenvironment in vitro, preserving cell-cell and cell-matrix interactions². Importantly, cell-sheet engineering is considered a scaffold-free, bottom-up approach in tissue engineering, because harvested sheets inherently contain ECM and cell-cell junctions, thereby representing an early form of 3D or-

ganization³,⁴,⁵. Modelling skin cells—especially fibroblasts and keratinocytes—using this technology is among the most promising strategies for producing functional skin tissue⁶.

Based on the cell-sheet approach, cells can be obtained as a continuous layer without disrupting intercellular connections and while preserving the ECM; this contributes to the creation of more robust and functional structures in tissue-engineering applications ⁷, ⁸. Given its effects on cell proliferation and differentiation, this technology offers not only structural but also biological advantages ⁷, ⁹. Although special materials, such as temperature-sensitive culture surfaces, are used in classical cell-sheet formation methods, these techniques are complex and costly. Therefore, cell-sheet production using L-AA emerges as a more practical and widely preferred alternative ¹⁰, ¹¹.

Research has shown that L-AA stimulates fibroblasts to synthesize collagen and enhances ECM production while promoting keratinocyte

Cite this article: Hatice Demir, Arzu Coleri Cihan. Comparative Analysis of Ascorbic Acid-Induced Cell Sheet Formation in HaCaT Keratinocytes and Human Dermal Fibroblasts. *Biomed. Res. Ther.* 2025; 12(10):7865-7875.

growth 12, 13, 14. In addition, ascorbic acid suppresses intracellular reactive oxygen species (ROS), exerts antioxidant effects, and supports cellular proliferation and DNA synthesis 15, 16. Previous studies have demonstrated that ascorbic acid supports fibroblast ECM production and COL1A1 expression ¹⁰, ¹⁷ and contributes to 3D co-culture systems involving fibroblasts and keratinocytes⁶. However, these studies either focused on stem-cell-derived sheets or complex skin equivalents without directly comparing keratinocyte and fibroblast responses under identical conditions. In this study, the effects of different cell densities and ascorbic acid concentrations on cell sheets obtained from HaCaT and HDF cells were evaluated comprehensively. Cellsheet formation was assessed by viability (MTT) and morphological (crystal violet) staining analyses, after which gene-expression levels were evaluated in selected groups using qRT-PCR. Accordingly, this study presents an original approach that aims to fill the aforementioned gap in the literature and to contribute to cell-sheet modelling. Furthermore, we emphasize that cell-sheet engineering itself represents a scaffold-free, bottom-up 3D ap proach, because harvested sheets contain ECM and cell-cell junctions, providing an intermediate level of tissue organization relative to classical monolayers³, ⁴, ⁵.

MATERIALS-METHODS

Cell Culture

In this study, the immortalized human keratinocyte line HaCaT (Cytion, 300493; passage 3) and the human dermal fibroblast line HDF (ATCC, PCS-201-010; passage 5) were employed. HDF cells were cultured in Dulbecco's Modified Eagle Medium (DMEM; Gibco, USA), whereas HaCaT cells were cultured in DMEM/F-12 (Gibco, USA). All media were supplemented with 10 % fetal bovine serum (Biological Industries, Cat. No. 04-001-1A), 2 mmol L^{-1} L-glutamine (Invitrogen, USA), and 100 U mL⁻¹ penicillin plus 100 μg mL⁻¹ streptomycin (Invitrogen, USA). Cells were incubated at 37 °C in a humidified atmosphere containing 5 % CO₂. Both lines were confirmed to be mycoplasma-free using the Microsart® AMP Mycoplasma Kit (Sartorius, SMB95-1001); representative agarose-gel electrophoresis results are shown in Supplementary Figure 1. HaCaT and HDF cells were seeded into 24-well plates at 5×10^4 or 1×10^5 cells cm⁻². Twenty-four hours after seeding, L-ascorbic acid (L-AA; Sigma-Aldrich, USA) was added as described below.

L-Ascorbic Acid (L-AA) Stock Preparation and Application

L-ascorbic acid (Sigma-Aldrich, USA) stock solutions were prepared at 10 mg mL $^{-1}$ in sterile PBS (pH 7.0), filtered through a 0.22-µm syringe filter, aliquoted under minimal light, and stored at $-20\,^{\circ}\mathrm{C}$. Working dilutions (25, 50, and 100 µg mL $^{-1}$) were prepared immediately before use and added to prewarmed medium. To minimize oxidation, all L-AA handling was performed under light protection, and aliquots were thawed only once. Culture medium was replaced every 48 h with freshly prepared L-AA-supplemented medium. Control groups without L-AA were also included. In total, 16 experimental groups were established, as summarised in Table 1.

Cell Sheet Formation and Evaluation

Cell morphology was monitored daily under an inverted phase-contrast microscope for 7 days. Half of the medium was replaced every 48 h, and at the end of the culture period sheet formation was evaluated microscopically. Formed sheets were gently washed with PBS, mechanically detached with a sterile pipette, and transferred to clean 6-well plates. To promote adhesion to a new surface, fresh medium was applied dropwise every 30 min for 3 h, after which the sheets were monitored for an additional 3 days. Cell sheet formation was defined according to both morphological and mechanical criteria: sheets were considered positive when they could be detached as an intact, continuous layer with a minimum diameter of ≥ 5 mm without enzymatic digestion, and when structural integrity was preserved under phase-contrast microscopy. Cultures that remained as fragile monolayers or detached in fragments were not classified as cell sheets. All groups $(0, 25, 50, 100 \,\mu \text{g mL}^{-1})$ were evaluated by MTT assay and phase-contrast microscopy. Groups that did not form cohesive sheets (25 μg mL⁻¹ and 100 μg mL^{-1}) were not processed for crystal violet staining or qRT-PCR.

MTT Analysis

Cell viability and metabolic activity were evaluated using the MTT assay on days 1, 3, 5, and 7 of the culture period. A 5 mg mL $^{-1}$ MTT solution was added to each well, and plates were incubated at 37 $^{\circ}$ C for 3 h in a 5 $^{\circ}$ CO $_{2}$ incubator. Following incubation, isopropanol containing 0.04 $^{\circ}$ (v/v) hydrochloric acid (Merck, Germany) was added to solubilize the formazan crystals 18 . Absorbance was measured on a microplate spectrophotometer (Thermo Scientific Multiskan GO, USA) at 570 nm with a reference wavelength of 690 nm.

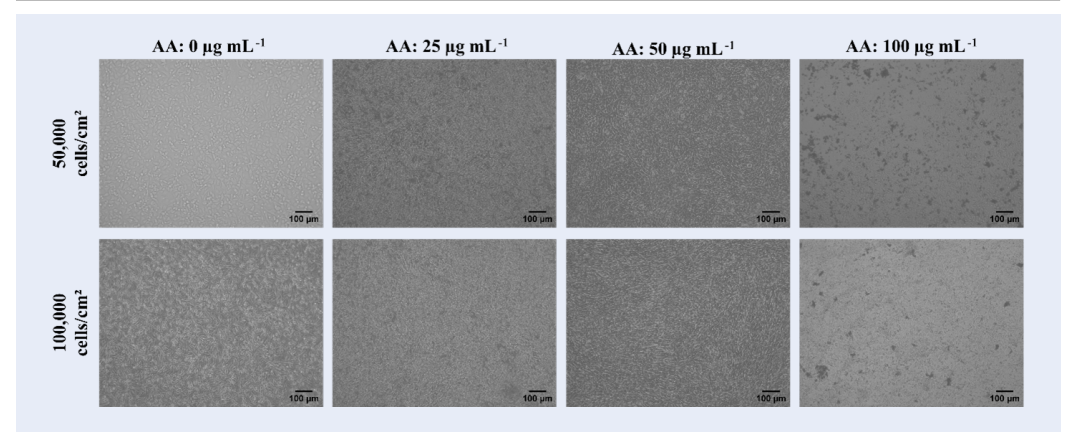


Figure 1: Effect of L-AA on fibroblast morphology. Inverted microscopy images showing the formation of HDF cell sheets under varying L-AA concentrations (0, 25, 50, and 100 μ g mL⁻¹) and two different seeding densities (50,000 and 100,000 cells/well). Clear sheet formation was observed at 50 μ g mL⁻¹ L-AA for both seeding densities, suggesting this concentration as optimal for sheet development. Images were captured on day 5. Scale bar = 100 μ ; magnification: 10×. Abbreviations: HDF, human dermal fibroblasts; L-AA, L-ascorbic acid.

Table 1: Experimental groups based on cell type, cell density, and ascorbic acid concentration

Cell Line	Cell Density (cells/cm²)	Ascorbic Acid Concentration ($\mu g m L^{-1}$)
HaCaT	50,000	0 (Control), 25, 50, 100
	100,000	0 (Control), 25, 50, 100
HDF	50,000	0 (Control), 25, 50, 100
	100,000	0 (Control), 25, 50, 100

Note: All groups were analyzed for viability (MTT) and morphology (phase-contrast microscopy). Cohesive sheet formation was observed only in human dermal fibroblasts (HDF) at 50 μg mL $^{-1}$ (50,000 cells/cm 2). Human keratinocytes (HaCaT) did not form sheets at any concentration. The 25 μg mL $^{-1}$ groups resembled controls, and 100 μg mL $^{-1}$ groups showed cytotoxicity; therefore, these were not subjected to crystal violet staining or quantitative real-time PCR (qRT-PCR).

Crystal Violet Staining

To evaluate cell morphology and proliferation, crystal violet staining was performed on days 3 and 7. Before staining, the culture medium was removed and the cells were fixed with a 1:1 acetone:methanol solution (Merck, Germany) for 10 min at room temperature. Fixed cells were stained with 0.1 % crystal violet (Sigma-Aldrich, USA) for 30 min at room temperature. After staining, excess dye was removed by washing with distilled water ¹⁹. Plates were airdried and examined with an inverted phase-contrast microscope (Zeiss, Germany) to assess morphology, proliferation, and adhesion.

Quantitative Real-Time PCR (qRT-PCR) Analysis

On day 7, gene expression analysis was performed to evaluate epidermal and dermal differentiation as

well as cell proliferation. Total RNA was isolated using the RNeasy Mini Kit (Qiagen, Germany), and 1 μg RNA per sample was reverse-transcribed with iScript™ Reverse Transcription Supermix (Bio-Rad, USA). For HDF cells, RNA was isolated from mechanically detached cohesive sheets (50 μ g mL⁻¹, 50 k seeding). For HaCaT cells, because no sheets were obtained, RNA was extracted from confluent adherent monolayers at the indicated seeding densities and L-AA concentrations. To assess epidermal differentiation, KRT14 and IVL transcripts were quantified in HaCaT cells; Ki-67 expression was determined to assess proliferation. In HDF cells, the extracellular matrix genes COL1A1, COL3A1, and FN1 were analysed. Relative quantification was performed using the 2-ΔΔCt method. GAPDH and ACTB served as reference genes and displayed stable expression across all groups. All qRT-PCR reactions were conducted with iTaq™ Universal SYBR® Green Supermix (Bio-Rad, USA) according to the manufacturer's instructions. Threshold cycle (Ct) values were recorded and relative expression levels calculated. All primers were newly designed to span exon-exon junctions and therefore avoid genomic DNA amplification; sequences were generated with NCBI Primer-BLAST based on RefSeq mRNA entries. Primer sequences and target gene information are summarised in Table 2.

Image Acquisition and Processing

All microscopic images were obtained with an inverted phase-contrast microscope (Zeiss, Germany) at 10× and 20× magnification. Scale bars were included in every panel and adjusted for clarity. Images were exported in TIFF format at 300 dpi. All illustrations are original and were generated during the course of this study. Only uniform adjustments of brightness and contrast were applied to entire images; no selective manipulations were performed. Macroscopic images of detached cell sheets were captured with a digital camera to illustrate gross morphology; consequently, no scale bar was applied.

Statistical Analysis

Data are presented as mean ± standard deviation (SD) from three independent experiments per group. HaCaT and HDF cell lines were evaluated separately. The effects of different L-AA concentrations and cell densities on cell viability and gene expression were analysed for each line. Individual and interactive effects of ascorbic acid concentration and cell density were examined by two-way analysis of variance (two-way ANOVA). When significance was detected, Tukey's multiple-comparison test was applied. Gene expression levels were calculated from Ct values using the $\Delta\Delta$ Ct method. Differences with p < 0.05 were considered statistically significant. Full numerical MTT data (raw absorbance values, mean ± SD, and post-hoc p-values) are provided in Supplementary Tables S1-S4.

RESULTS

Cell Sheet Formation and Evaluation

Cell-sheet formation was assessed in selected groups by culturing HaCaT and HDF cells at various seeding densities in the presence of escalating concentrations of L-ascorbic acid (L-AA). Cell morphology was inspected daily under an inverted microscope for 7 days, and sheet formation was

scored according to the degree of confluence (Figures 1 and 2). In HDF cultures seeded at 50 000 cells cm⁻² and supplemented with 50 μg mL⁻¹ L-AA, a compact, well-defined sheet became apparent on day 7 (Figure 3). These sheets satisfied the predefined criteria of intact detachment (≥ 5 mm diameter) and microscopic structural integrity. Following gentle mechanical detachment, the sheets were successfully transferred onto fresh culture substrates, to which they adhered and remained stable during subsequent incubation. High-resolution microscopy revealed a dense, homogeneous architecture throughout both central and peripheral regions, confirming structural integrity (Figure 3A,B). Representative images acquired on day 3 are shown in Figure 3C to illustrate early morphological changes and proliferation. A macroscopic photograph obtained after successful transfer of an intact sheet further demonstrates its cohesiveness (Figure 3D). Annotations highlight the uniform cell distribution and extracellular-matrix-rich appearance of the con-

Unlike HDFs, HaCaT cells failed to generate discernible sheets under any condition during the 7day observation period. The highest proliferation rate was recorded in the group seeded at 100 000 cells cm $^{-2}$ and treated with 50 μg mL $^{-1}$ L-AA. All cultures were maintained by exchanging half of the medium every 48 h to satisfy metabolic demands (Figure 2). Enhanced proliferation in the 100 000cell wells receiving 50 μg mL⁻¹ L-AA implies a progrowth, non-differentiating effect of this dose. Conversely, cytotoxicity-manifested by decreased cell density and morphological alterations-was evident at 100 μ g mL⁻¹. At 25 μ g mL⁻¹, both cell types resembled untreated controls and failed to form cohesive sheets. Because of the pronounced toxicity, the 100 μ g mL⁻¹ groups were omitted from crystalviolet and qRT-PCR assays, although viability and morphology data are presented in the main figures.

MTT Assay

An MTT assay performed on days 1, 3, 5, and 7 demonstrated that the metabolic activity of both cell types was dependent on L-AA concentration and seeding density. In HDFs, metabolic activity peaked on day 5 in the 50 μg mL $^{-1}$ groups, with viability significantly exceeding that of the 25 and 100 μg mL $^{-1}$ groups (p < 0.05). In contrast, viability declined markedly in cultures exposed to 100 μg mL $^{-1}$ L-AA, indicating dose-dependent toxicity (Figure 4). In HaCaT cells, proliferation increased from day 3 onward in high-density cultures supplemented

Table 2: Primer Sequences, Target Genes and Accession Number

Gene	Function / Relevance	Target Cell Type	Primer Sequence (5' $ ightarrow$ 3')	Product Size (bp)	RefSeq Accession [GenBank]
COL1A1	Dermal ECM protein (Type I collagen)	HDF	F: CCCCGAGGCTCTGAAGGT R: ACCAGGTTCACCGCTGTTAC	188	NM_000088.4
COL3A1	Dermal ECM protein (Type III collagen)	HDF	F:TAAAGGCGAAATGGGTCCCG R:GGCACCATTCTTACCAGCCT	202	NM_000090
FN1	Fibronectin, ECM glycoprotein	HDF	F:CCCGGAATGTAGGACAAGA R:TGCCTGCTGGTCTTTTCAG	175	NM_212482.3
KRT14	Basal keratinocyte marker (Keratin 14)	HaCaT	F:GCAGCATCCAGAGATGTGAC R:TATTGATTGCCAGGGAGGGG	145	NM_000526.5
IVL	Terminal epidermal differentiation marker	НаСаТ	F:GCCTTACGTGAGTCTGGTTGA R:TGCTTTGATGGGACCTCCAC	178	NM_005547.4
Ki-67	Proliferation marker	HaCaT	F: GGATCGTCCCAGTGGAAGAG R: CAAAACAAGCAGGTGCTGAGG	163	NM_002417.5
GAPDH	Housekeeping gene (internal control)	HaCaT, HDF	F:CCGCATCTTCTTTTGCGTCG R:GCCCAATACGACCAAATCCT	120	NM_002046.7
ACTB (β- actin)	Housekeeping gene (internal control)	HaCaT, HDF	F: AGCAAGCAGGAGTACGATGAG R: AAAGGGTGTAAAACGCAGCTC	120	NM_001101.5

Abbreviations: ECM, extracellular matrix; HDF, human dermal fibroblasts; HaCaT, human keratinocyte cell line; bp, base pairs.

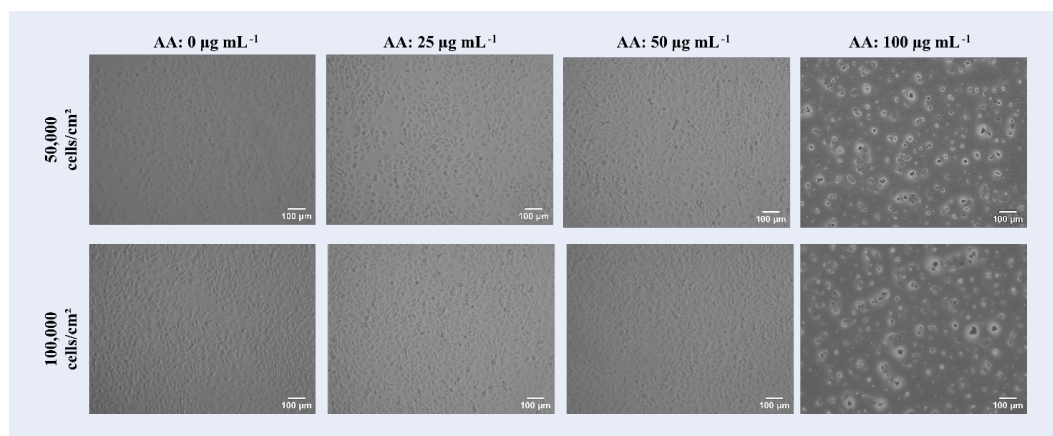


Figure 2: Effect of L-AA on keratinocyte m orphology. Inverted microscopy images of HaCaT cell cultures treated with varying concentrations of L-AA at two different seeding densities. Images were captured on day 5. Scale bar = $100 \,\mu$; magnification: $10 \times$. Abbreviations: HDF, human dermal fibroblasts; L-AA, L-ascorbic acid.

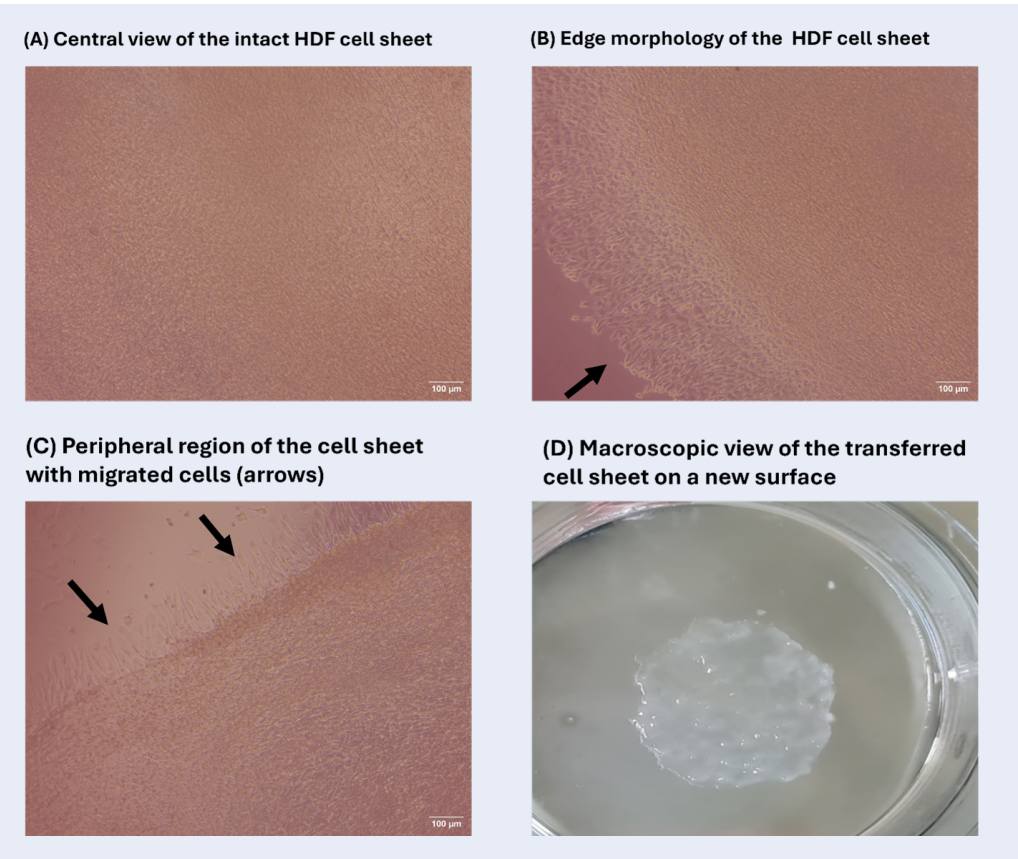


Figure 3: Morphology of the HDF cell sheet under optimal conditions. Morphological characterization of the HDF cell sheet under optimal conditions (50 μ g mL $^{-1}$ L-AA and 50,000 cells/cm² seeding density). Scale bar = 100 μ ; magnification: 10×. **Abbreviations:** HDF, human dermal fibroblasts; L-AA, L-ascorbic acid.

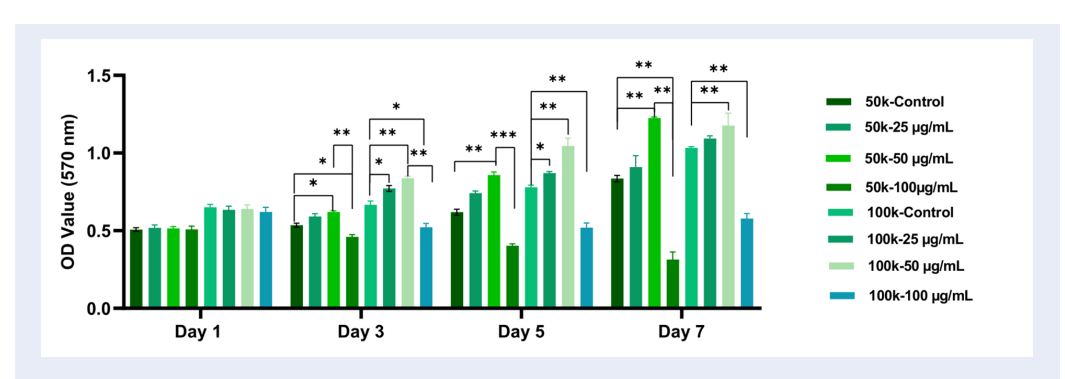


Figure 4: MTT analysis results of HDF cells cultured with different concentrations of L-AA. HDF cells were seeded at densities of 50,000 and 100,000 cells/cm² and applied with 0-100 μg mL $^{-1}$ L-AA. Cell viability was assessed on days 1, 3, 5, and 7 using the MTT assay (n = 3). Data are presented as mean ± SD. The group applied with 50 μg mL $^{-1}$ L-AA at 50,000 cells/cm² exhibited the highest metabolic activity by day 7 (p <0.05), whereas exposure to 100 μg mL $^{-1}$ resulted in a significant reduction in viability, indicating a dose-dependent cytotoxic effect. Complete raw values and statistical outputs are presented in Supplementary Tables S1. **Abbreviations:** HDF, human dermal fibroblasts; HaCaT, human keratinocyte cell line; L-AA, L-ascorbic a cid; MTT, 3-(4,5-Dimethylthiazol-2-yl)-2,5-Diphenyltetrazolium Bromide.

with 50 μ g mL⁻¹ L-AA, whereas the 100 μ g mL⁻¹ groups showed no such rise (Figure 5). Overall, low-to moderate L-AA concentrations promoted time-dependent increases in viability, but this effect was abrogated at 100 μ g mL⁻¹. The magnitude of the metabolic response depended on both L-AA dose and initial cell number.

Crystal-Violet Staining

Crystal-violet staining was used to visualise sheet morphology and cell density. After 7 days, only the HDF group seeded at 50 000 cells cm⁻² and treated with 50 µg mL⁻¹ L-AA produced a uniform, compact sheet that retained its morphology after transfer (Figure 6). Preservation of central-zone integrity confirmed successful sheet formation. Stepwise supplementation of culture medium at 30-min intervals facilitated re-spreading of the temporarily contracted sheet on the new substrate.

Gene-Expression Profiling by qRT-PCR

Because HaCaT cells did not form sheets, RNA was extracted from confluent monolayers, whereas HDF RNA was isolated from detached sheets. Expression data were normalised to the geometric mean of GAPDH and ACTB, which remained stable across all conditions. Relative expression was calculated by the 2– $\Delta\Delta$ Ct method. In HDF sheets (50 000 cells cm $^{-2}$, 50 µg mL $^{-1}$ L-AA, day 7) COL1A1, COL3A1, and FN1 were significantly up-regulated versus untreated controls (p < 0.05), with COL1A1 displaying the greatest fold increase (Figure 7A), indicating enhanced extracellular-matrix synthesis under optimal L-AA supplementation.

In confluent HaCaT monolayers (100 000 cells cm⁻², 50 µg mL⁻¹ L-AA), KRT14, IVL, and Ki-67 transcripts were elevated on day 7, with IVL showing the most pronounced induction (Figure 7B). These findings suggest that, in keratinocytes, 50 µg mL⁻¹ L-AA stimulates proliferation and early differentiation without promoting sheet cohesion. Collectively, L-AA modulates gene expression and functional outcomes in a dose- and cell-type-specific manner: fibroblasts respond by producing cohesive, ECM-rich sheets, whereas keratinocytes exhibit increased proliferation and differentiation marker expression in the absence of sheet formation.

DISCUSSION

In this study, cell sheet formation was investigated systematically at two cell-seeding densities (50,000

and 100,000 cells cm⁻²) and across a range of L-AA concentrations $(0-100 \mu g mL^{-1})$ in HDF fibroblasts and HaCaT keratinocytes. Although the capacity of L-AA to induce collagen synthesis 20, 21, regulate extracellular-matrix (ECM) production²², and support cellular organization23 has been well documented, holistic experimental models comparing these effects across different cell densities and doses remain limited. Moreover, whereas most earlier studies focused on fibroblast sheet induction, the differential response of keratinocytes has not been systematically addressed. By analyzing both cell types under identical conditions, our study provides novel comparative insights and highlights cell-type-specific responses to L-AA that have not been reported in previous static-culture studies, thereby adding experimental and conceptual novelty to scaffold-free, bottom-up cell-sheet engineer-

Previous studies have shown that L-AA supports cell-sheet formation in tissues such as bone 24, cartilage²⁵, cornea²⁶, and periodontal ligament ¹⁷, ²⁷. However, detailed analyses of fibroblast-based sheets are scarce: therefore, our work clarifies the optimal parameters for fibroblast sheet generation. The data indicate that the most effective sheet formation in HDFs was obtained with a seeding density of 50,000 cells cm⁻² and 50 μ g mL⁻¹ L-AA. Under these conditions, both cellular viability increased significantly and ECM deposition improved. This finding demonstrates the dual role of L-AA in cell-sheet engineering-simultaneously supporting metabolic activity and promoting ECM formation. In contrast, at the higher concentration of 100 μg mL⁻¹, viability declined and sheet architecture was disrupted from day 3 onward, consistent with reports that supraphysiological L-AA elicits cytotoxicity through oxidative stress, H2O2 generation, and possible pH shifts 28, 29. Although catalase-rescue assays were not performed, we recognize this limitation and note that the precise toxic mechanism warrants further investigation.

Crystal-violet staining corroborated these observations, revealing high cell density and well-organized, transferable sheets in the 50 μg mL $^{-1}$ group. Sheets were compact, uniform, and mechanically stable, making them transferable without enzymatic treatment—an important advantage over existing methods that often require temperature-responsive surfaces or enzymatic detachment $^3,^{30-32}$. Morphometric analysis across central and peripheral zones confirmed preservation of the spindle-shaped fibroblast phenotype, with pronounced alignment

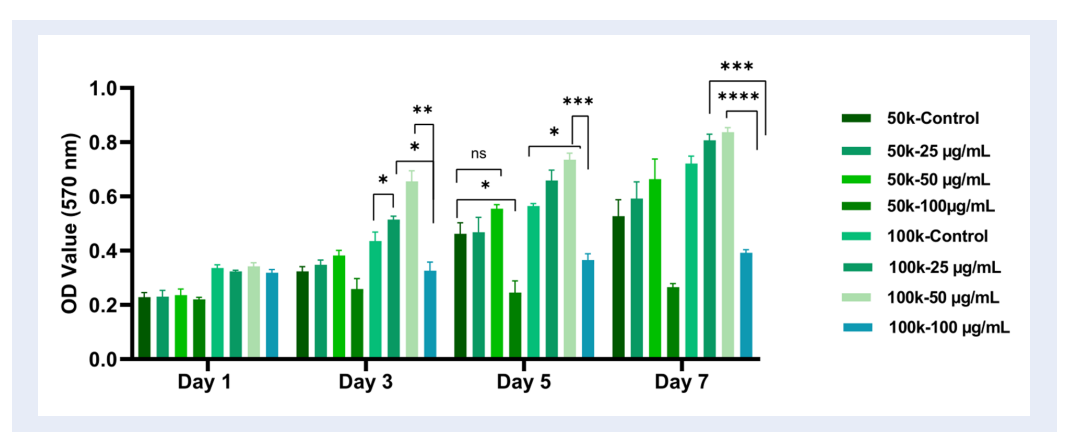


Figure 5: MTT analysis results of HaCaT cells cultured at different L-AA concentrations. HaCaT keratinocytes were seeded at densities of 50,000 and 100,000 cells/cm² and L-AA was applied in the range of $0-100 \, \mu \mathrm{g} \, \mathrm{mL}^{-1}$. MTT analysis was performed on days 1, 3, 5 and 7 (n=3) and absorbance was measured at $570 \, \mathrm{nm}$. A significant increase in cell viability was observed in the $50 \, \mu \mathrm{g} \, \mathrm{mL}^{-1}$ L-AA group, especially at a density of $100,000 \, \mathrm{cells/cm^2}$, on day 7. On the other hand, it was determined that the $100 \, \mu \mathrm{g} \, \mathrm{mL}^{-1}$ concentration decreased cell viability and showed a toxic effect starting from day 3 . Complete raw values and statistical outputs are presented in Supplementary Tables S3. **Abbreviations:** HDF, human dermal fibroblasts; HaCaT, human keratinocyte cell line; L-AA, L-ascorbic acid; MTT, $3-(4,5-\mathrm{Dimethylthiazol-}2-\mathrm{yl})-2,5-\mathrm{Diphenyltetrazolium}$ Bromide.

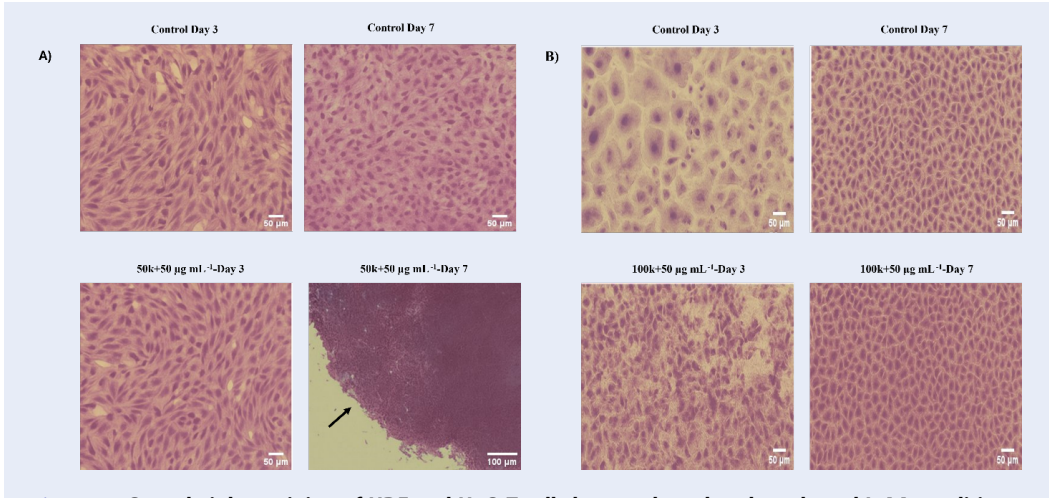


Figure 6: Crystal violet staining of HDF and HaCaT cell sheets cultured under selected L-AA conditions. Representative crystal violet-stained images of cell sheets formed by (A) HDF and (B) HaCaT cells under selected L-AA concentrations. Images were captured on days 3 and 7. Optimal conditions promoted the development of dense and cohesive cell sheets by day 7, with preserved morphology and structural integrity after mechanical transfer. Continued expansion and reattachment post-transfer confirmed viability and sheet stability. Scale bars = $50 \mu m$; magnification: $20 \times$ and $100 \mu m$; m agnification: $10 \times$. Abbreviations: HDF, human dermal fibroblasts; HaCaT, human keratinocyte cell line; L-AA, L-ascorbic acid.

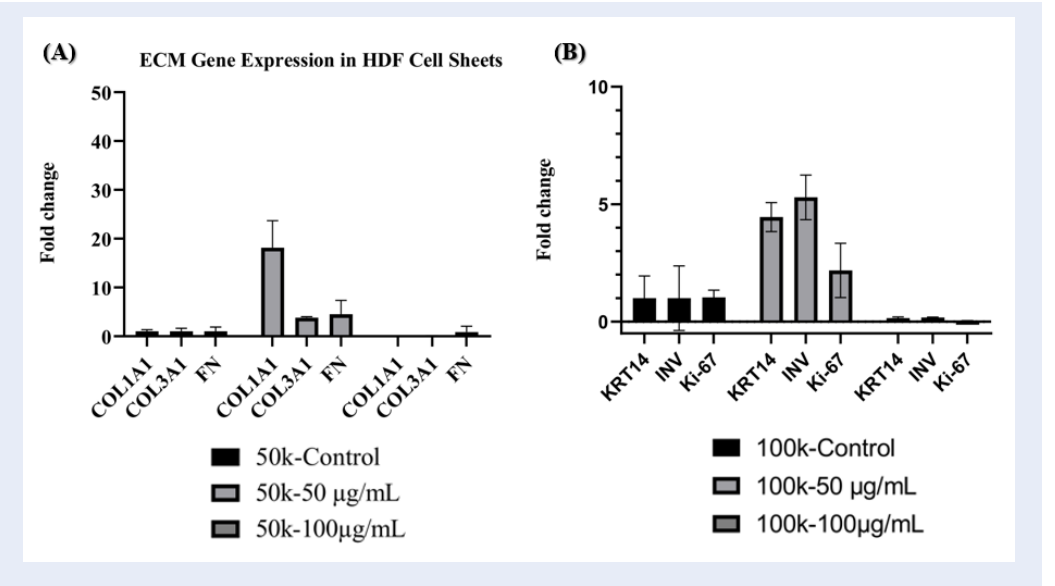


Figure 7: Relative gene expression in HDF and HaCaT cell sheets cultured under optimal L-AA conditions. (A) In HDF cells seeded at 50,000 cells/cm² and applied with $50\,\mu\mathrm{g}\,\mathrm{mL}^{-1}$ L-AA, a significant upregulation of COL1A1, COL3A1, and FN1 genes was observed compared to the unapplied control (p < 0.05), indicating enhanced ECM production and dermal matrix formation. (B) In HaCaT cells seeded at 100,000 cells/cm² with $50\,\mu\mathrm{g}\,\mathrm{mL}^{-1}$ L-AA treatment, increased expression levels of KRT14, IVL and Ki-67 were detected, with IVL involucrin showing the highest fold change, suggesting promoted epidermal differentiation and proliferative a ctivity. HaCaT samples represent confluent adherent monolayers, not detached s heets. Data were normalized to the arithmetic mean of GAPDH and ACTB reference genes. Abbreviations: HDF, human dermal fibroblasts; HaCaT, human keratinocyte cell line; L-AA, L-ascorbic acid; ECM, extracellular matrix; COL1A1, Collagen type I alpha 1 chain; COL3A1, Collagen type III alpha 1 chain; FN1, Fibronectin 1; KRT14, Keratin 14; IVL, Involucrin.

and orientation—hallmarks of active cell–cell and cell–matrix interactions. These findings agree with evidence that fibroblasts guide the organization of collagen-rich ECM ³³, ³⁴, ³⁵.

By contrast, HaCaT cultures failed to develop compact, cohesive sheets within the same period and exhibited a less organized morphology. This attenuated response suggests that keratinocytes differ from fibroblasts in their dependence on L-AA and may require longer culture times or additional growth factors and signaling cues to establish a stable ECM ³⁶. Consequently, keratinocytebased sheets will likely benefit from advanced three-dimensional or co-culture strategies, underscoring the translational value of our comparative model for engineered skin.

Finally, qRT-PCR analysis paralleled the morphological data. Dermal genes COL1A1, COL3A1, and FN1 were significantly up-regulated in the optimal 50 $\mu g\ mL^{-1}$ condition, confirming augmented ECM synthesis at the transcriptional level. In keratinocytes, however, differentiation markers such as IVL were more strongly induced than structural

genes, further emphasizing the novelty of our head-to-head approach. Because both HaCaT and HDF are immortalized lines, these results should be regarded as proof-of-concept; validation with patient-derived primary cells is necessary before clinical translation. Collectively, these molecular findings reinforce the necessity of optimizing both L-AA concentration and seeding density for successful sheet formation. Beyond these endpoints, cell-sheet engineering represents a scaffold-free, bottom-up three-dimensional strategy that differs fundamentally from traditional monolayer culture and broadens the toolkit of regenerative medicine.

CONCLUSION

As a result, HDF cell sheets cultured at a density of 50,000 cells cm $^{-2}$ and treated with 50 $\mu g\ mL^{-1}$ L-AA emerged as the optimal condition, exhibiting superior morphological integrity, cell viability, mechanical stability, and ECM-related gene expression. These findings provide a strong biological rationale for incorporating such sheets into co-culture systems, wound-healing models, or full-thickness

three-dimensional skin equivalents in future studies. Moreover, the study underscores the critical influence of both dose-response relationships and cell-density optimization in skin tissue engineering. Future work that combines these sheets with dynamic culture systems, growth factors, or advanced scaffold a rchitectures is likely to further enhance their clinical relevance. The primers designed herein to evaluate gene expression during epidermal and dermal differentiation and cell proliferation will also serve as a foundation for subsequent investigations. Collectively, L-AA-supported fibroblast sheets may be regarded as biofunctional building blocks that recapitulate the cellular microenvironment and facilitate functional tissue fabrication for next-generation regenerative applications.

ABBREVIATIONS

ACTB: β-actin; cm²: Square centimeters; COL1A1: Collagen type I alpha 1 chain; COL3A1: Collagen type III alpha 1 chain; DMEM: Dulbecco's Modified Eagle Medium; ECM: Extracellular matrix; FBS: Fetal bovine serum; FN1: Fibronectin 1; GAPDH: Glyceraldehyde-3-phosphate dehydrogenase; HaCaT: Human keratinocyte cell line; HDF: Human dermal fibroblasts; IVL: Involucrin; Ki-67: A proliferation marker; KRT14: Keratin 14; L-AA: L-ascorbic acid; MTT: 3-(4,5-Dimethylthiazol-2-yl)-2,5-Diphenyltetrazolium Bromide; PBS: Phosphate-buffered s aline; q RT-PCR: Qu antitative real-time polymerase chain reaction; μg mL⁻¹: Micrograms per milliliter

ACKNOWLEDGMENTS

We thank to the Scientific and Technological Research Council of Türkiye (TÜBİTAK project code: 119C208) for the PhD scholarship support provided within the framework of TÜBİTAK 2244 - Industrial Doctorate Programme. We also thank Sentebiolab Biotechnology Inc. for their contribution to the PhD scholarship.

Author's contributions

Hatice Demir conceptualized the study, designed the methodology, conducted the experiments, curated and analyzed the data, created the visualizations, and wrote the original draft of the manuscript. Arzu Çöleri Cihan contributed to the conceptualization and methodology, supervised the research, reviewed and edited the manuscript, and was responsible for project administration and funding acquisition. All authors read and approved the final manuscript.

Funding

None.

Availability of data and materials

Data and materials used and/or analyzed during the current study are available from the corresponding author on reasonable request.

Ethics approval and consent to participate

Not applicable.

Consent for publication

Not applicable.

Declaration of generative AI and AIassisted technologies in the writing process

The authors declare that they have not used generative AI (a type of artificial intelligence technology that can produce various types of content including text, imagery, audio and synthetic data. Examples include ChatGPT, NovelAI, Jasper AI, Rytr AI, DALLE, etc) and AI-assisted technologies in the writing process before submission.

Competing interests

The authors declare that they have no competing interests

REFERENCES

- Randall MJ, Jüngel A, Rimann M, Wuertz-Kozak K. Advances in the biofabrication of 3D skin in vitro: healthy and pathological models. Front Bioeng Biotechnol. 2018 Oct;6:154. PMID: 30430109. Available from: https://doi.org/10.3389/fbioe.2018. 00154.
- Yamato M, Okano T. Cell sheet engineering. Mater Today. 2004;7(5):42–47. Available from: https://doi.org/10.1016/S1369-7021(04)00234-2.
- Haraguchi Y, Shimizu T, Yamato M, Okano T. Scaffold-free tissue engineering using cell sheet technology. RSC Adv. 2012;2(6):2184–2190. Available from: https://doi.org/10.1039/ c2ra00704e.
- Kim K, Bou-Ghannam S, Okano T. Cell sheet tissue engineering for scaffold-free three-dimensional (3D) tissue reconstruction. Methods Cell Biol. 2020;157:143–167. PMID: 32334713. Available from: https://doi.org/10.1016/bs.mcb.2019.11.020.
- Hu D, Li X, Li J, Tong P, Li Z, Lin G, et al. The preclinical and clinical progress of cell sheet engineering in regenerative medicine. Stem Cell Res Ther. 2023 Apr;14(1):112. PMID: 37106373. Available from: https://doi.org/10.1186/s13287-023-03340-5.
- Cerqueira MT, Pirraco RP, Martins AR, Santos TC, Reis RL, Marques AP. Cell sheet technology-driven re-epithelialization and neovascularization of skin wounds. Acta Biomater. 2014 Jul;10(7):3145–3155. PMID: 24650971. Available from: https://doi.org/10.1016/j.actbio.2014.03.006.
- Ng KW, Hutmacher DW. Reduced contraction of skin equivalent engineered using cell sheets cultured in 3D matrices. Biomaterials. 2006 Sep;27(26):4591–4598. PMID: 16720038. Available from: https://doi.org/10.1016/j.biomaterials.2006.04.020.

- Lin YC, Grahovac T, Oh SJ, Ieraci M, Rubin JP, Marra KG. Evaluation of a multi-layer adipose-derived stem cell sheet in a full-thickness wound healing model. Acta Biomater. 2013 Feb;9(2):5243–5250. PMID: 23022891. Available from: https://doi.org/10.1016/j.actbio.2012.09.028.
- Badylak SF. The extracellular matrix as a biologic scaffold material. Biomaterials. 2007 Sep;28(25):3587–3593.
 PMID: 17524477. Available from: https://doi.org/10.1016/j. biomaterials.2007.04.043.
- Wei F, Qu C, Song T, Ding G, Fan Z, Liu D, et al. Vitamin C treatment promotes mesenchymal stem cell sheet formation and tissue regeneration by elevating telomerase activity. J Cell Physiol. 2012 Sep;227(9):3216–3224. PMID: 22105792. Available from: https://doi.org/10.1002/jcp.24012.
- Trottier V, Marceau-Fortier G, Germain L, Vincent C, Fradette J.
 IFATS collection: using human adipose-derived stem/stromal
 cells for the production of new skin substitutes. Stem Cells.
 2008 Oct;26(10):2713–2723. PMID: 18617689. Available from:
 https://doi.org/10.1634/stemcells.2008-0031.
- Karna E, Szoka L, Huynh TY, Palka JA. Proline-dependent regulation of collagen metabolism. Cell Mol Life Sci. 2020 May;77(10):1911–1918. PMID: 31740988. Available from: https://doi.org/10.1007/s00018-019-03363-3.
- Tajima S, Pinnell SR. Ascorbic acid preferentially enhances type I and III collagen gene transcription in human skin fibroblasts. J Dermatol Sci. 1996 Mar;11(3):250–253. PMID: 8785178. Available from: https://doi.org/10.1016/0923-1811(95)00640-0.
- Catani MV, Savini I, Rossi A, Melino G, Avigliano L. Biological role of vitamin C in keratinocytes. Nutr Rev. 2005 Mar;63(3):81–90. PMID: 15825810. Available from: https://doi.org/10.1111/j.1753-4887.2005.tb00125.x.
- Kim JE, Jin DH, Lee SD, Hong SW, Shin JS, Lee SK, et al. Vitamin C inhibits p53-induced replicative senescence through suppression of ROS production and p38 MAPK activity. Int J Mol Med. 2008 Nov;22(5):651–655. PMID: 18949386.
- Taniguchi M, Arai N, Kohno K, Ushio S, Fukuda S. Anti-oxidative and anti-aging activities of 2-O-α-glucopyranosyl-L-ascorbic acid on human dermal fibroblasts. Eur J Pharmacol. 2012 Jan;674(2-3):126–131. PMID: 22119379. Available from: https://doi.org/10.1016/j.ejphar.2011.11.013.
- Ashok K, Thomas B, Manjappa AB, Shetty J, Rao S, Basavarajappa MK, et al. Characterization and evaluation of ascorbic acid-induced cell sheet formation in human periodontal ligament stem cells: an in vitro study. J Oral Biosci. 2021 Dec;63(4):429–435. PMID: 34666146. Available from: https://doi.org/10.1016/j.job.2021.10.002.
- Buranaamnuay K. The MTT assay application to measure the viability of spermatozoa: A variety of the assay protocols. Open Vet J. 2021;11(2):251–269. PMID: 34307082. Available from: https://doi.org/10.5455/OVJ.2021.v11.i2.9.
- Feoktistova M, Geserick P, Leverkus M. Crystal violet assay for determining viability of cultured cells. Cold Spring Harb Protoc. 2016;2016(4):pdb.prot087379. Available from: https:// doi.org/10.1101/pdb.prot087379.
- Murad S, Grove D, Lindberg KA, Reynolds G, Sivarajah A, Pinnell SR. Regulation of collagen synthesis by ascorbic acid. Proc Natl Acad Sci USA. 1981 May;78(5):2879–2882. PMID: 6265920. Available from: https://doi.org/10.1073/pnas.78.5.2879.
- Pinnell SR. Regulation of collagen biosynthesis by ascorbic acid: a review. Yale J Biol Med. 1985;58(6):553-559. PMID: 3008449
- D'Aniello C, Cermola F, Patriarca EJ, Minchiotti G. Vitamin C in stem cell biology: impact on extracellular matrix homeostasis and epigenetics. Stem Cells Int. 2017;2017:8936156.
 PMID: 28512473. Available from: https://doi.org/10.1155/2017/8936156.

- Guo X, Hutcheon AE, Melotti SA, Zieske JD, Trinkaus-Randall V, Ruberti JW. Morphologic characterization of organized extracellular matrix deposition by ascorbic acid-stimulated human corneal fibroblasts. Invest Ophthalmol Vis Sci. 2007 Sep;48(9):4050-4060. PMID: 17724187. Available from: https: //doi.org/10.1167/iovs.06-1216.
- Akahane M, Shimizu T, Kira T, Onishi T, Uchihara Y, Imamura T, et al. Culturing bone marrow cells with dexamethasone and ascorbic acid improves osteogenic cell sheet structure. Bone Joint Res. 2016 Nov;5(11):569–576. PMID: 27881440. Available from: https://doi.org/10.1302/2046-3758. 511.BJR-2016-0013.R1.
- Sato Y, Mera H, Takahashi D, Majima T, Iwasaki N, Wakitani S, et al. Synergistic effect of ascorbic acid and collagen addition on the increase in type 2 collagen accumulation in cartilage-like MSC sheet. Cytotechnology. 2017 Jun;69(3):405–416. PMID: 26572654. Available from: https://doi.org/10.1007/s10616-015-9924-3.
- Hasenzahl M, Müsken M, Mertsch S, Schrader S, Reichl S. Cell sheet technology: influence of culture conditions on in vitrocultivated corneal stromal tissue for regenerative therapies of the ocular surface. J Biomed Mater Res B Appl Biomater. 2021 Oct;109(10):1488–1504. PMID: 33538123. Available from: https: //doi.org/10.1002/jbm.b.34808.
- Iwata T, Yamato M, Washio K, Ando T, Okano T, Ishikawa
 Cell sheets for periodontal tissue engineering. Curr Oral Health Rep. 2015;2(4):252–256. Available from: https://doi.org/ 10.1007/s40496-015-0063-x.
- Kim TJ, Byun JS, Kwon HS, Kim DY. Cellular toxicity driven by high-dose vitamin C on normal and cancer stem cells. Biochem Biophys Res Commun. 2018 Feb;497(1):347–353.
 PMID: 29432735. Available from: https://doi.org/10.1016/j.bbrc. 2018.02.083.
- Szarka A, Kapuy O, Lőrincz T, Bánhegyi G. Vitamin C and cell death. Antioxid Redox Signal. 2021 Apr;34(11):831–844.
 PMID: 32586104. Available from: https://doi.org/10.1089/ars. 2019.7897.
- Imashiro C, Shimizu T. Fundamental technologies and recent advances of cell-sheet-based tissue engineering. Int J Mol Sci. 2021 Jan;22(1):425. PMID: 33401626. Available from: https:// doi.org/10.3390/ijms22010425.
- Li M, Ma J, Gao Y, Yang L. Cell sheet technology: a promising strategy in regenerative medicine. Cytotherapy. 2019 Jan;21(1):3–16. PMID: 30473313. Available from: https://doi.org/10.1016/j.jcyt.2018.10.013.
- Matsuda N, Shimizu T, Yamato M, Okano T. Tissue engineering based on cell sheet technology. Adv Mater. 2007;19(20):3089– 3099. Available from: https://doi.org/10.1002/adma.200701978.
- Berry DP, Harding KG, Stanton MR, Jasani B, Ehrlich HP. Human wound contraction: collagen organization, fibroblasts, and myofibroblasts. Plast Reconstr Surg. 1998 Jul;102(1):124–131. PMID: 9655417. Available from: https://doi.org/10.1097/00006534-199807000-00019.
- Fernandez-Madrid F, Noonan S, Riddle J. The "spindle-shaped" body in fibroblasts: intracellular collagen fibrils. J Anat. 1981 Mar;132(Pt 2):157–166. PMID: 7275796.
- Kanta J. Collagen matrix as a tool in studying fibroblastic cell behavior. Cell Adh Migr. 2015;9(4):308–316. PMID: 25734486. Available from: https://doi.org/10.1080/19336918. 2015.1005469.
- Joshi A, Nuntapramote T, Brüggemann D. Self-assembled fibrinogen scaffolds support cocultivation of human dermal fibroblasts and HaCaT keratinocytes. ACS Omega. 2023 Feb;8(9):8650–8663. PMID: 36910955. Available from: https://doi.org/10.1021/acsomega.2c07896.